Journal of Inflammation Research

Dovepress
Taylor & Francis Group

Open Access Full Text Article

ORIGINAL RESEARCH

Integrated Multi-Omic Analysis Reveals Causal Relationships and Causal Mechanisms of Peripheral Lymphocyte-Driven Remodeling in the Intrahepatic Immune Microenvironment of Early-Stage MAFLD

Shiqi Guo[1,2], Zhengrui Li[3,4], Zhenlong Han[1,2], Yunpeng Ge[1,2], Haowei Shi[1,2], Yangyang Zheng[1,2], Wendan Tan[1,5], Cheng Xing[1], Zhichao Li[2,6], Yao Li[1], Jinghai Song[1]

[1]Department of General Surgery, Department of Hepato-Bilio-Pancreatic Surgery, Beijing Hospital, National Center of Gerontology, Institute of Geriatric Medicine, Chinese Academy of Medical Sciences, Beijing, People's Republic of China; [2]Chinese Academy of Medical Sciences & Peking Union Medical College, Beijing, People's Republic of China; [3]Shanghai Jiao Tong University School of Medicine, Shanghai, People's Republic of China; [4]Department of Surgery, Shanghai Ninth People's Hospital, Shanghai, People's Republic of China; [5]Peking University Fifth School of Clinical Medicine, Beijing, People's Republic of China; [6]National Cancer Center/National Clinical Research Center for Cancer /Cancer Hospital, Chinese Academy of Medical Sciences and Peking Union Medical College, Beijing, People's Republic of China

Correspondence: Jinghai Song, Department of General Surgery, Department of Hepato-bilio-pancreatic Surgery, Beijing Hospital, National Center of Gerontology, Institute of Geriatric Medicine, Chinese Academy of Medical Sciences, Beijing, People's Republic of China, Tel +86-13701330496, Email jhaisong2003@126.com

Background: Metabolic dysfunction-associated fatty liver disease (MAFLD), the most common chronic liver disease worldwide, is characterized as a chronic inflammatory disease within an altered immune microenvironment. Investigating the relationship between peripheral blood parameters and intrahepatic immune remodeling is significant for developing non-invasive diagnostic tools and targeted immunotherapies for early MAFLD. This study aimed to investigate the causal relationships and underlying mechanisms between peripheral blood cell indices and intrahepatic immune microenvironment remodeling in early-stage MAFLD.

Methods: We performed bidirectional mendelian randomization analyses to assess the causal effects of peripheral blood cell traits on MAFLD risk. Mediation mendelian randomization was applied to identify key inflammatory mediators. Hepatic immune cell recruitment pathways were explored by integrating mendelian randomization findings with bulk RNA sequencing data. Single-cell RNA sequencing of mouse models that replicate metabolic syndrome-associated MAFLD pathology was employed to characterize lymphocyte-driven pathways. Key findings were validated using an independent public single-cell RNA sequencing dataset derived from human peripheral blood mononuclear cells and an independent public single-cell RNA sequencing dataset from a non-genetically modified murine model.

Results: (1) Bidirectional Mendelian randomization revealed a unidirectional causal effect of elevated peripheral lymphocyte count on disease risk. (2) Mediation analysis implicated Cd5-mediated inflammatory pathways in this association. (3) Integration of mendelian randomization and bulk transcriptomic data linked lymphocytes to hepatic recruitment pathways. (4) Single-cell RNA sequencing of MAFLD models identified a novel Itgb1^{+}Cd5^{+}Cd4^{+}T cell subset enriched in diseased livers. These cells interact with hepatic Vcam1^{high}Mmp12^{+}Kupffer cells via Vcam1-Itgb1 signaling, initiating inflammation. (5) This pathogenic cell subset and interaction were conserved in an independent, non-genetically modified murine model. Furthermore, a corresponding Itgb1^{+}Cd5^{+}Cd4^{+}T cell population was identified in the peripheral blood mononuclear cells of human MAFLD patients.

Conclusion: We innovatively established that peripheral T lymphocytes exhibit a positive causal relationship with MAFLD development, mediated by Cd5 expression levels. Furthermore, liver-resident Vcam1^{high}Kupffer cells may facilitate immune microenvironment remodeling in early MAFLD by recruiting Itgb1^{+}Cd5^{+}Cd4^{+}T cells through the Vcam1-Itgb1 adhesion pathway.

Keywords: metabolic dysfunction-associated fatty liver disease, inflammatory proteins, lymphocyte, T cells, macrophage

Received: 13 June 2025
Accepted: 17 November 2025
Published: 3 December 2025

Introduction

Metabolic dysfunction-associated fatty liver disease (MAFLD) has now surpassed viral hepatitis as the most prevalent chronic liver disease worldwide,[1,2] currently affecting over 30% of the global population and showing a steadily increasing prevalence.[3] Patients with MAFLD exhibit persistent metabolic disturbances and chronic inflammation driven by multifaceted inflammatory triggers. The pathogenesis involves not only intrahepatic mechanisms, such as lipid overload, lipotoxicity, and oxidative stress but also extrahepatic systems, including the gut-liver axis and adipose tissue, through coordinated multi-organ crosstalk. Together, these hepatic and systemic factors drive the characteristic inflammation-mediated MAFLD progression.[4,5] Dysregulation of the hepatic immune microenvironment is a central driver of inflammation and disease progression in MAFLD.[6] However, current treatments—including the FDA-approved Resmetirom for MASH and other late-stage metabolic-targeted drugs—show limited efficacy.[7–9] This underscores the promising therapeutic potential of strategies that modulate intrahepatic inflammation or combine metabolic and immune targets. Consequently, a deeper investigation into the disrupted immune homeostasis in MAFLD is of paramount importance.[4,10–12]

Notably, MAFLD is a systemic chronic inflammatory disease. The peripheral circulation serves as a critical interface between the liver and extrahepatic organs, dynamically modulating the hepatic immune microenvironment through the exchange of immune cells and soluble mediators.[13–16] Therefore, understanding the interplay between peripheral immunity and intrahepatic immune alterations is crucial for developing non-invasive diagnostics and identifying novel therapeutic targets. Emerging evidence suggests that alterations in peripheral lymphocyte counts (Lympho)—particularly functional and proportional changes in cytotoxic T cells, $Cd4^+$ T cells, and natural killer (NK) cells—correlate strongly with MAFLD progression.[17] However, existing cross-sectional studies limit causal inferences regarding Lympho-MAFLD relationships and obscure the mechanistic links between peripheral Lympho and intrahepatic inflammatory responses. Additionally, the substantial genetic predisposition in MAFLD pathogenesis highlights the need to investigate hereditary influences on hepatic and systemic immune regulation.[18] Building upon this foundation, this study integrates genome-wide association studies (GWAS), Mendelian randomization (MR), bulk RNA sequencing (bulk RNA-seq), single-cell RNA sequencing (scRNA-seq), and metabolic syndrome-associated MAFLD models to integratively investigate the causal relationship between peripheral hematological parameters and intrahepatic immune microenvironment remodeling during early MAFLD and the molecular mechanisms underlying Lympho-driven MAFLD development. These findings will enhance the current understanding of peripheral-intrahepatic immune homeostasis in MAFLD pathogenesis and provide a theoretical foundation for advancing non-invasive diagnostic biomarkers and refining early-stage targeted immunomodulatory therapeutic strategies.

Materials and Methods

GWAS Data Collection and Processing

This study first employed bidirectional and mediation MR analyses to establish causal relationships between peripheral blood cell traits and MAFLD and to identify key inflammatory mediators. Single-nucleotide polymorphisms (SNPs) significantly associated with the prioritized blood cell traits were extracted from genome-wide association study summary statistics. These SNPs were integrated with bulk RNA-seq data to calculate a quantitative "MR score" for each sample. Differential gene expression and Gene Set Enrichment Analysis (GSEA) were then performed using the MR score. Finally, scRNA-seq was used to identify the specific cell subpopulations and cell-cell communication networks associated with the MR-prioritized mediators, elucidating the role of peripherally-derived immune cells in remodeling the early MAFLD hepatic immune microenvironment. The overall study design is depicted in Figure 1. Genetic associations for MAFLD were sourced from publicly available GWAS catalogs (ebi-a-GCST90054782), encompassing 377,988 individuals. All cases were confirmed via clinical laboratory testing and physician diagnosis.[19] The study included individuals of European ancestry to minimize potential confounding effects related to race, thereby controlling for genetic and environmental factors, ensuring a more homogeneous sample, and providing a clearer understanding of the contributions of circulatory hematological cells to MAFLD. Summary statistics for 15 hematological traits were sourced from the Blood Cell Consortium (BCX) meta-analysis, comprising 562,242 participants of European

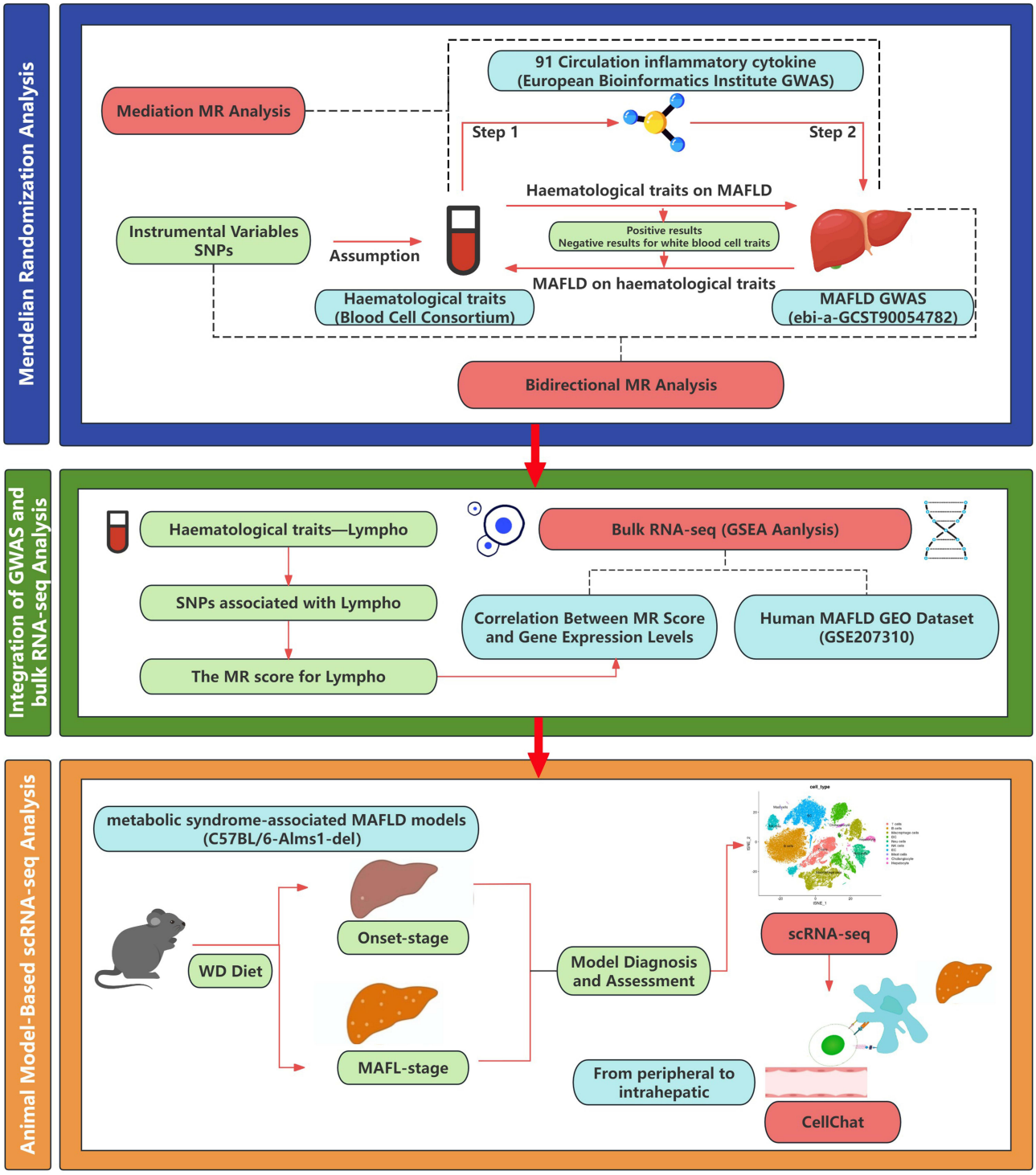

Figure 1 Study Roadmap.
Abbreviations: MAFLD, Metabolic dysfunction-associated fatty liver disease; Lympho, lymphocyte count; scRNA-seq, single-cell RNA sequencing; SNP, single nucleotide polymorphisms; MR, Mendelian randomization; GESA, Gene Set Enrichment Analysis; WD, Western diet.

ancestry. GWAS data for 91 inflammatory proteins were obtained from the European Bioinformatics Institute (EBI) GWAS Catalog, with information from 11 cohorts involving 14,824 individuals of European ancestry. These data were based on protein quantitative trait loci analysis for these plasma proteins. The full summary statistics for each protein GWAS are available through the Cambridge PHPC Proteins (https://www.phpc.cam.ac.uk/ceu/proteins) and the EBI

GWAS Catalog (accession numbers GCST90274758 to GCST90274848). Detailed information regarding all genetic correlation results is available in the Supplementarydata.

The Alms1-Deficient Murine Model for Investigating Metabolic Syndrome-Associated MAFLD

Alms1 knockout in C57BL/6 mice (C57BL/6-Alms1-del) induces hyperphagia, obesity predisposition, and glucose-lipid metabolic dysregulation, with Western diet (WD)-induced MAFLD pathological features demonstrating high clinical relevance to human disease.[20] This study utilized a gene-edited model featuring an 11-bp deletion in exon 8, causing premature translational termination (generated by GemPharmatech Co., Ltd., Jiangsu, China), with experiments conducted under standardized conditions (24°C, 55% humidity, 12-h light/dark cycle). To model the transition from metabolic susceptibility to early fatty liver disease and investigate associated immunological events, we established two experimental groups for comparison: an "Onset" group and a "MAFL" group. Seven-week-old male mice (n = 6) were randomly assigned to either group (n = 3 per group). The Onset group received standard chow for 2 weeks followed by a 1-week mixed diet containing 30% WD, while the MAFL group was maintained on a 100% WD throughout the study. The WD (GAN diet, D09100310 formula) contained 40% fat, 20% fructose, and 2% cholesterol.[21] Serum biochemical parameters were systematically measured using a Hitachi 3500 automated clinical chemistry analyzer (JM1123-776230). The metabolic dysregulation phenotype was assessed by measuring alanine aminotransferase (ALT), aspartate aminotransferase (AST), total cholesterol (TCHOL), triglycerides (TG), high-density lipoprotein cholesterol (HDL), and low-density lipoprotein cholesterol (LDL). Terminal assessments revealed that the Onset group livers displayed normal gross morphology with histopathology showing scattered microvesicular fat droplets (<5% hepatic involvement) and absence of macrovesicular steatosis, whereas the MAFL group exhibited intra-abdominal visceral fat accumulation, hepatomegaly with yellowish discoloration, elevated serum lipids, and mild fasting hyperglycemia, alongside histopathological findings of ≥5% macrovesicular steatosis without significant lobular inflammation or hepatocyte ballooning, consistent with MAFLD diagnostic criteria. Histopathological analysis and image acquisition were performed using a light microscope (Model: OLYMPUS CX23). All animal experimental procedures were conducted in accordance with the National Standards of the People's Republic of China, Laboratory animal—Guideline for ethical review of animal welfare (GB/T 35892–2018), and were approved by the Institute of Zoology, Chinese Academy of Sciences (Approval No. IOZ-IACUC-2024-194).

Isolation of Primary Murine Liver Non-Parenchymal Cells

(1) Isolation of Liver Non-Parenchymal Cells (NPC): Fresh hepatic tissue was enzymatically dissociated using a Liver Non-Parenchymal Cell Dissociation Kit (Miltenyi Biotec, 130–105-807) coupled with mechanical disruption via a gentleMACS™ Dissociator (Miltenyi, 130–093-235) for 36 min 12s, with all post-dissociation procedures maintained on ice. (2) Purification of NPCs: Residual hepatocyte and vascular tissue debris were subsequently removed using a Debris Removal Solution (Miltenyi, 130–109-398), followed by erythrocyte lysis with Hybri-Max™ Mild RBC Lysis Buffer (Sigma, R7757). Cell aggregates were dissociated through sequential treatment with DNase I solution and EDTA solution. (3) Rigorous Quality Control Criteria: A 10 μL quality control aliquot was stained with viability dye and analyzed using the BD Rhapsody™ Single-Cell Analyzer, with qualified samples defined by cell viability >90%, aggregate rate <5%, cellular density 500–800 cells/μL, and absence of macroscopic impurities. (4) Single-Cell Capture and Library Preparation: Following secondary validation, antibody-tagged samples were processed for whole transcriptome amplification (WTA) and sample multiplexing kit (SMK) library preparation, scaled according to target cell capture requirements.

Instrumental Variable Selection

To ensure data quality, variants with a genotype call rate of <98% across all samples were excluded. The mean sequencing depth exceeded 20×. Population stratification was assessed using principal component analysis, and related individuals were excluded based on identity-by-descent estimates to maintain population homogeneity in the European ancestry cohort. Additional quality control measures were implemented, including a minimum mean depth of 8×;

exclusion of SNPs exhibiting significant deviation from Hardy–Weinberg equilibrium ($P < 1 \times 10^{-5}$) in controls, as extreme deviations may indicate genotyping errors; and removal of SNPs with excessive genotyping failure rates and genotype call rates >98%. The cohort encompassed both common and low-frequency variants, retaining those with a minor allele frequency ≥ 0.5% to enhance the coverage of genetic instruments while ensuring the reliability of effect size estimates for subsequent analyses.

Two-Sample Bidirectional MR Analyses

MR analyses were conducted to examine whether 15 specific hematological traits causally influence MAFLD. For positive forward MR results, reverse MR analysis was conducted to confirm the unidirectional causal relationship between specific hematological traits and MAFLD. The inverse-variance weighted (IVW) method was used as the primary analysis, supported by MR-Egger regression, weighted median, simple median, and weighted mode methods to account for potential pleiotropy and provide robust estimates. The IVW method combines effect estimates of the IVs, assuming no pleiotropy, while the MR-Egger and weighted median methods serve as sensitivity analyses to detect and adjust for pleiotropy.

Mediation MR Analysis

The mediation analysis employed a two-step MR approach to investigate the mechanistic pathways through which circulating Blood Cell Consortium (BCX) influence MAFLD. First, the causal effects of BCX on inflammatory factors were estimated via two-sample MR (β(A)). Subsequently, independent causal effects of inflammatory factors on MAFLD were assessed, ensuring mediator-outcome associations were unconfounded by exposure (β(B)). The mediation effect was calculated as β(A) × β(B). BCX total effects on MAFLD were derived from prior MR analyses, with direct effects computed as total effect – mediation effect. Mediation proportions were quantified as *(mediation effect / total effect) × 100%*. Inflammatory factors were classified as potential mediators in the blood cell-to-MAFLD pathway only if causal triangulation was satisfied: (1) exposure (BCX)-outcome MAFLD, (2) mediator (inflammatory factors)-outcome, and (3) exposure-mediator relationships were all causally supported. Levels of evidence were stratified based on the completeness of causal chains across these associations.

Heterogeneity and Pleiotropy Assessments

Heterogeneity and pleiotropy analyses were conducted to assess the robustness of the findings. Cochran's Q test was utilized to evaluate heterogeneity among SNPs, with significant heterogeneity indicating variability in IV effects. The MR-Egger intercept test was employed to detect directional pleiotropy, where a significant intercept indicated pleiotropy. Additionally, the Pleiotropy RESidual Sum and Outlier (MR-PRESSO) test was utilized to identify and correct outliers, ensuring MR results' reliability. Detailed information regarding all genetic correlation results is available in the Supplementary data.

Integration of GWAS and Bulk RNA-Seq Analysis

Thirteen samples with raw FASTQ files from the GEO dataset GSE207310 were downloaded, comprising seven samples diagnosed with nonalcoholic fatty liver (NAFL) and six samples diagnosed with Nonalcoholic Steatohepatitis (NASH). All diagnoses were histopathologically confirmed by liver biopsy, with NASH specifically defined by the presence of steatosis (≥1), lobular inflammation (≥1), and ballooning degeneration (≥1) according to the NAFLD Activity Score (NAS).[22] The raw FASTQ files were mapped to the human GRCh38 reference assembly using STAR (version 2.7.6a). The GTF annotation file (version 102) was downloaded from Ensembl and used for gene annotation in STAR. Duplicate reads were removed using GATK (version 4.2.0). Gene-level read counts were obtained using htseqcount (version 0.13.5). Gene expression data were normalized using the variance stabilizing transformation (VST) implemented in the DESeq2 package. Germline variants were extracted using GATK HaplotypeCaller in gVCF mode. SNPs relevant to MR were extracted from the output VCF files. We extracted SNPs significantly associated with lymphocyte count from the MR analysis along with their effect sizes (beta). For each sample in the GSE207310 dataset, a quantitative "Lymphocyte MR Score" was calculated using the formula: score = (beta1 × SNP1) + (beta2 × SNP2) +. + (betan × SNPn). Finally, we computed Spearman correlation coefficients between the Lymphocyte MR Score and the VST-normalized expression of

all genes. This generated a ranked gene list based on correlation strength, which was used as input for Gene Set Enrichment Analysis (GSEA) against the Gene Ontology (GO) database, performed with the clusterProfiler package.

scRNA-Seq Analysis

Single-cell RNA sequencing analysis was performed using the filtered gene-barcode matrix generated from BD Rhapsody™ as input for Seurat (v.4.2.2). Analysis commenced with liver non-parenchymal cell samples from Onset (n=3) and MAFL (n=3) groups. After removing doublets and low-quality cells, 73,470 cells expressing >500 genes and 29,316 transcripts detected in≥3 cells were retained for downstream processing. Following standardized preprocessing, logarithmic normalization was implemented via the "LogNormalize" algorithm. Highly variable genes (n=2000) were selected through computational feature selection. Dimensionality reduction employed principal component analysis (PCA) for biological variation capture and UMAP for 2D visualization. Cell clustering utilized a graph-based approach, integrating shared nearest-neighbor networks with modularity-optimized community detection, applying resolution=0.2 for global clustering. Subpopulation refinement employed resolution=0.8 for T cells and 0.5 for macrophages during manual annotation. Visualization tools (t-SNE, UMAP, violin plots, bar charts, circular plots, bubble plots, feature plots, heatmaps) were generated using R. Functional enrichment analyses included KEGG, GO, and GSEA pathways through R packages ("enrichKEGG," "enrichGO," "enrichGSEA"). Cell-cell communication analysis was conducted via CellChat, integrating transcriptomic profiles with curated ligand-receptor databases while applying stringent statistical thresholds (empirical $p<0.01$) for interaction validation. We downloaded and processed public single-cell transcriptomic datasets GSE267033 and GSE129516, primarily using Seurat (v5.1.0) and CellChat (v2.1.2). Both datasets underwent an identical preprocessing workflow: cells were retained if they expressed between 200 and 4000 genes (nFeature_RNA) and had a mitochondrial gene percentage (percent.mt) below 20%. The IntegrateLayers function was used for batch correction and data integration, followed by cell type annotation using established marker genes. For GSE267033, $CD4^+$ T cells were subsequently extracted for subpopulation analysis. For GSE129516, T cells and macrophages were extracted for subpopulation characterization. All studies involving animal and human data (including publicly available datasets) in this research were approved by the Research Ethics Committee of Beijing Hospital (Approval No. 2025BJYYEC-KY155-01).

Results

Causal Association Between Peripheral Lympho Levels and MAFLD: A Bidirectional Two-Sample MR Analysis

To investigate whether peripheral hematological parameters are causally linked to MAFLD and to identify specific contributing blood-based biomarkers, a bidirectional two-sample MR analysis was first conducted to systematically assess causal associations between 15 clinically relevant hematological traits and MAFLD risk. In the ebi-a-GCST90054782 dataset, Lympho (odds ratio [OR] = 1.131, 95% confidence interval [CI]: 1.012–1.264, P = 0.029), hematocrit (HCT) (OR = 1.244, 95% CI: 1.074–1.440, P = 0.004), HGB (OR = 1.283, 95% CI: 1.114–1.479, P = 0.001), and mean corpuscular hemoglobin concentration (MCHC) (OR = 1.167, 95% CI: 1.013–1.345, P = 0.032) were associated with a significantly increased MAFLD risk, while red cell distribution width (RDW) exhibited a protective effect (OR=0.878, 95% CI=0.793–0.972, P=0.012) (Table 1). Lympho was identified as the sole peripheral leukocyte parameter causally linked to MAFLD incidence. These risk and protective associations were further corroborated by sensitivity analyses using MR-Egger, simple median, weighted median, and weighted mode methods (Figure 2a–c). To ensure robustness, heterogeneity and pleiotropic analyses were conducted. Leave-one-out analysis indicated that results were not driven by a single SNP (Supplementary Figure 1). Sensitivity analyses using scatter plots and outlier removal revealed no significant heterogeneity in the positive associations (Supplementary Figures 2 and 3). No significant heterogeneity was detected among positive associations, supporting instrument variable consistency. Additionally, MR-Egger intercept analysis did not detect significant directional pleiotropy, indicating that the results are unlikely to be affected by horizontal pleiotropy. To further clarify the causal directionality between these circulating parameters and MAFLD risk, reverse MR analysis was performed. Based on reverse MR results, the five positive hematological traits were unidirectionally associated with MAFLD, and no causal relationship was found between other leukocyte markers and MAFLD (all P>0.05; Table 2). These findings collectively

Table 1 Significant MR Results Between Hematological Parameters and MAFLD

Outcome	Exposure	Method	N.SNPs	Beta	SE	p Value	OR (95% CI)
MAFLD	Lympho	IVW	484	0.123	0.057	0.029	1.131 (1.012–1.264)
		MR Egger	484	0.047	0.123	0.703	1.048 (0.824–1.333)
		Simple median	484	0.154	0.08	0.053	1.167 (0.998–1.363)
		Weighted median	484	0.127	0.083	0.128	1.135 (0.964–1.336)
		Weighted mode	484	0.136	0.133	0.306	1.146 (0.883–1.486)
MAFLD	HCT	IVW	448	0.218	0.075	0.004	1.244 (1.074–1.440)
		MR Egger	448	0.308	0.144	0.034	1.361 (1.025–1.806)
		Simple median	448	0.141	0.089	0.112	1.151 (0.967–1.370)
		Weighted median	448	0.227	0.096	0.018	1.255 (1.039–1.514)
		Weighted mode	448	0.293	0.14	0.037	1.340 (1.018–1.764)
MAFLD	HGB	IVW	456	0.249	0.072	0.001	1.283 (1.114–1.479)
		MR Egger	456	0.296	0.134	0.028	1.345 (1.034–1.750)
		Simple median	456	0.185	0.088	0.035	1.204 (1.014–1.430)
		Weighted median	456	0.185	0.095	0.053	1.203 (0.998–1.450)
		Weighted mode	456	0.297	0.118	0.012	1.346 (1.069–1.695)
MAFLD	MCHC	IVW	231	0.155	0.072	0.032	1.167 (1.013–1.345)
		MR Egger	231	0.15	0.123	0.224	1.161 (0.913–1.477)
		Simple median	231	0.163	0.107	0.127	1.177 (0.954–1.452)
		Weighted median	231	0.148	0.105	0.157	1.160 (0.945–1.425)
		Weighted mode	231	0.222	0.11	0.044	1.248 (1.007–1.547)
MAFLD	RDW	IVW	427	−0.131	0.052	0.012	0.878 (0.793–0.972)
		MR Egger	427	−0.087	0.089	0.331	0.917 (0.770–1.092)
		Simple median	427	−0.061	0.076	0.423	0.941 (0.810–1.092)
		Weighted median	427	−0.097	0.073	0.186	0.907 (0.786–1.048)
		Weighted mode	427	−0.08	0.085	0.35	0.923 (0.781–1.091)

Notes: P-values from the IVW MR test were adjusted using the Benjamini-Hochberg false discovery rate correction, and the threshold was set to.05.

Abbreviations: IVW, inverse-variance-weighted; MR, Mendelian randomization; OR, odds ratio; SE, standard error; SNP, single nucleotide polymorphism; Lympho, lymphocyte count; HGB, hemoglobin concentration; MCHC, mean corpuscular hemoglobin concentration; HCT, hematocrit; RDW, red blood cell distribution width.

support a unidirectional "hematological trait→MAFLD" causal paradigm, suggesting that elevated peripheral Lympho may exacerbate hepatic pathology through systemic inflammatory mechanisms.

CD5 Mediates The Inflammatory Pathway Linking Peripheral Lympho to MAFLD

Building upon the cascade hypothesis of "peripheral immune cells → inflammatory mediators → target organ injury," a two-step mediation MR analysis was conducted to examine the mediating pathway from peripheral hematological traits to MAFLD. First, IVs from circulating hematological traits were used to estimate the causal effect of exposure on potential mediator variables, such as inflammatory factors. It was found that Lympho, MCHC, and other hematological traits were associated with MAFLD risk. Second, the causal effect of mediator variables on NAFLD risk was estimated, identifying causal evidence for the influence of T-cell surface glycoprotein Cd5 (Cd5) levels on MAFLD risk (β=0.047, proportion mediated=38.47%) (Figure 2d). While C-X-C motif chemokine 9 (Cxcl9) showed partial mediation in univariable analysis (indirect effect=0.023, P=0.038), its contribution was comparatively minor. The absence of significant heterogeneity across positive associations confirmed instrument variable consistency. These findings suggest that Cd5 may serve as a pivotal molecular node linking peripheral T-lymphocytosis to hepatic inflammatory cascades in MAFLD pathogenesis.

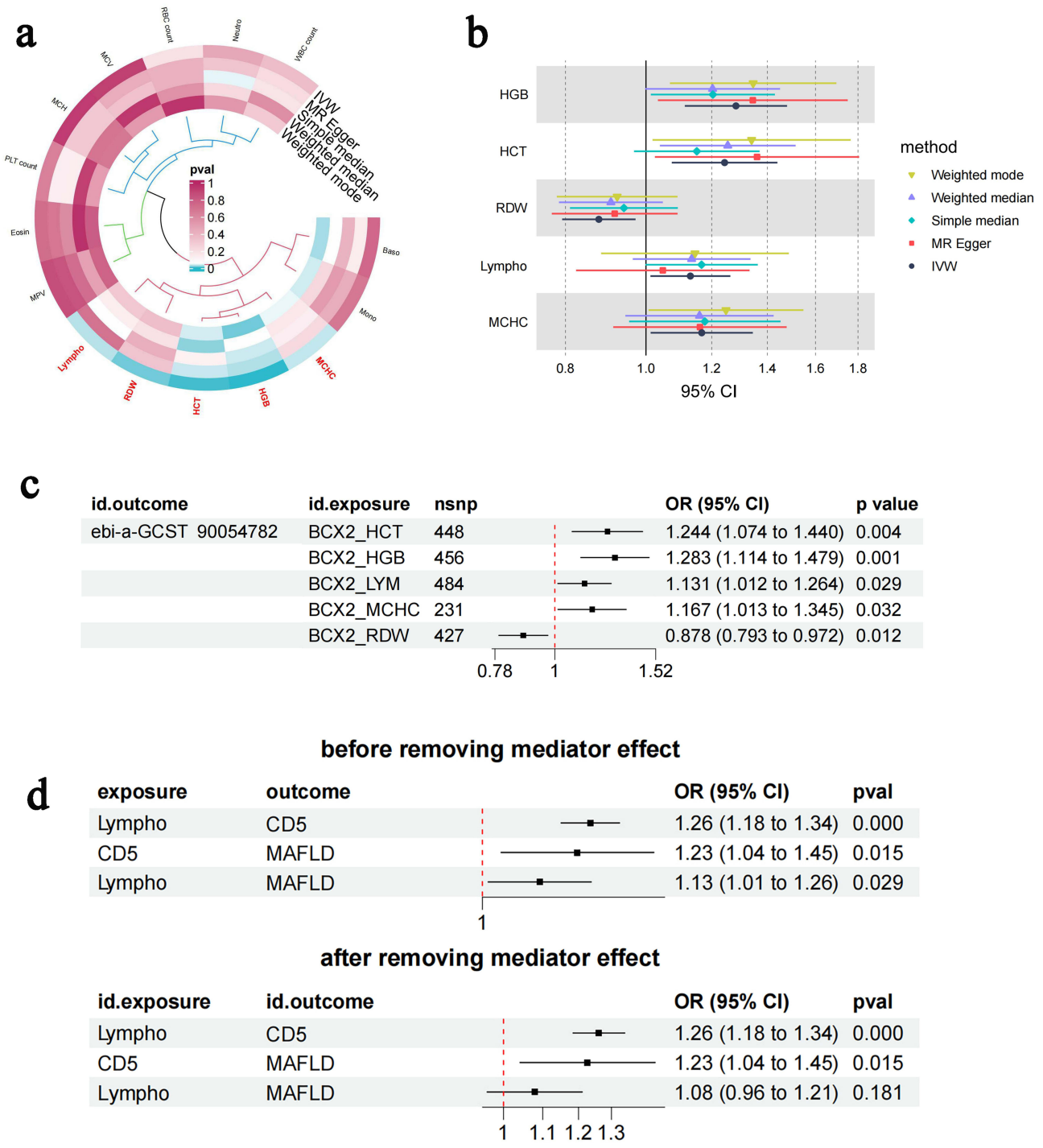

Figure 2 Bidirectional MR and Mediation MR analysis of peripheral Lympho and MAFLD Causality (**a**) MR circos exposure for the relationship of blood cell traits to MAFLD. (**b**) MR forest exposure for the relationship of blood cell traits to MAFLD. (**c**) MR forest for the relationship of blood cell traits to MAFLD. (**d**) Mediation MR analysis identifies T-cell surface glycoprotein Cd5 (Cd5) as a causal mediator between lymphocyte levels and metabolic dysfunction-associated fatty liver disease.
Abbreviations: IVW, inverse-variance-weighted; OR, odds ratio; Lympho or LYM, lymphocyte count; HGB, hemoglobin concentration; MCHC, mean corpuscular hemoglobin concentration; HCT, hematocrit; RDW, red blood cell distribution width.

Integrated bulkRNA-Seq and MR Analysis Reveal Peripheral T Lymphocyte Migration to the Liver

To further investigate the mechanistic link between lymphocyte count and MAFLD, and to evaluate whether individuals with a genetically determined high peripheral lymphocyte count exhibit specific transcriptional signatures in liver tissue,

Table 2 Reverse MR Results Between Hematological Parameters and MAFLD

Outcome	Exposure	Method	N.SNPs	Beta	SE	p Value	OR (95% CI)
Lympho	MAFLD	IVW	7	0.021	0.065	0.744	1.021(0.899–1.160)
		MR Egger	7	−0.123	0.242	0.633	0.885(0.551–1.420)
		Weighted median	7	0.016	0.052	0.761	1.016(0.917–1.126)
		Simple median	7	0.022	0.068	0.742	1.023(0.895–1.169)
		Weighted mode	7	0.001	0.053	0.992	1.001(0.902–1.110)
HCT	MAFLD	IVW	7	−0.025	0.041	0.539	0.975(0.901–1.056)
		MR Egger	7	0.236	0.122	0.111	1.266(0.997–1.608)
		Weighted median	7	0.011	0.047	0.813	1.011(0.921–1.110)
		Simple median	7	0.008	0.054	0.876	1.008(0.907–1.122)
		Weighted mode	7	−0.02	0.054	0.728	0.981(0.882–1.090)
HGB	MAFLD	IVW	7	−0.011	0.039	0.773	0.989(0.917–1.067)
		MR Egger	7	0.247	0.122	0.099	1.280(1.008–1.625)
		Weighted median	7	0.001	0.045	0.988	1.001(0.916–1.093)
		Simple median	7	−0.037	0.058	0.517	0.963(0.860–1.079)
		Weighted mode	7	0.037	0.061	0.562	1.038(0.922–1.169)
MCHC	MAFLD	IVW	7	0.02	0.044	0.66	1.020(0.935–1.112)
		MR Egger	7	−0.04	0.169	0.823	0.961(0.689–1.339)
		Weighted median	7	0.049	0.049	0.321	1.050(0.953–1.157)
		Simple median	7	0.024	0.061	0.691	1.024(0.910–1.154)
		Weighted mode	7	0.042	0.051	0.437	1.043(0.944–1.153)
RDW	MAFLD	IVW	7	−0.065	0.036	0.074	0.937(0.872–1.006)
		MR Egger	7	−0.134	0.129	0.346	0.875(0.680–1.126)
		Weighted median	7	−0.078	0.049	0.116	0.925(0.840–1.019)
		Simple median	7	−0.071	0.061	0.243	0.931(0.826–1.050)
		Weighted mode	7	−0.097	0.057	0.141	0.908(0.812–1.015)
WBC	MAFLD	IVW	7	0.011	0.068	0.874	1.011(0.885–1.154)
		MR Egger	7	−0.212	0.239	0.417	0.809(0.506–1.294)
		Weighted median	7	−0.008	0.051	0.879	0.992(0.899–1.096)
		Simple median	7	0.081	0.065	0.214	1.084(0.955–1.231)
		Weighted mode	7	−0.032	0.049	0.538	0.968(0.879–1.066)
Nrutro	MAFLD	IVW	7	−0.007	0.046	0.875	0.993(0.908–1.086)
		MR Egger	7	−0.178	0.158	0.311	0.837(0.614–1.140)
		Weighted median	7	−0.043	0.048	0.370	0.958(0.872–1.052)
		Simple median	7	−0.039	0.064	0.546	0.962(0.848–1.091)
		Weighted mode	7	−0.064	0.048	0.236	0.938(0.853–1.032)
Mono	MAFLD	IVW	7	0.011	0.049	0.831	1.011(0.918–1.113)
		MR Egger	7	−0.058	0.188	0.77	0.944(0.653–1.363)
		Weighted median	7	−0.026	0.051	0.618	0.975(0.881–1.078)
		Simple median	7	0.112	0.067	0.094	1.118(0.981–1.275)
		Weighted mode	7	−0.017	0.052	0.754	0.983(0.887–1.089)
Eosin	MAFLD	IVW	7	−0.012	0.062	0.845	0.988(0.875–1.116)
		MR Egger	7	0.082	0.237	0.743	1.085(0.682–1.726)
		Weighted median	7	−0.003	0.054	0.954	0.997(0.896–1.109)
		Simple median	7	−0.014	0.064	0.831	0.986(0.87–1.118)
		Weighted mode	7	0.013	0.056	0.82	1.013(0.908–1.131)
Baso	MAFLD	IVW	7	0.082	0.044	0.063	1.086(0.996–1.184)
		MR Egger	7	0.171	0.166	0.351	1.186(0.857–1.643)
		Weighted median	7	0.051	0.05	0.305	1.053(0.954–1.162)
		Simple median	7	0.055	0.062	0.376	1.056(0.935–1.193)
		Weighted mode	7	0.056	0.05	0.299	1.058(0.960–1.166)

we constructed a polygenic score for lymphocyte count based on GWAS-significant SNPs. This score was tested for genome-wide associations with the hepatic transcriptomic profiles of MAFLD patients. GSEA analysis was subsequently employed to identify biological pathways enriched for this genetic predisposition. Bulk RNA-seq was integrated with MR-prioritized lymphocyte-associated SNP loci, performing differential expression analysis via volcano plots and GSEA. To further investigate the mechanistic underpinnings linking Lympho to MAFLD pathogenesis, bulk RNA-seq data were integrated with MR-associated SNPs prioritized through GWAS for Lympho traits, followed by differential gene expression analysis and GSEA. Upregulated genes were significantly enriched in migration- and motility-related biological processes (BP), including "positive regulation of cell adhesion," "ameboid-type cell migration," and "leukocyte migration," with molecular functions (MF) such as "cadherin binding" (Figure 3a, b and Supplementary Figure 4). These findings indicate that the causal effects of peripheral Lympho on MAFLD pathogenesis are mediated through transcriptional reprogramming of T lymphocyte hepatic recruitment, suggesting that migratory transcriptional signatures in T lymphocytes may drive disease progression.

scRNA-Seq Reveals Early Hepatic Infiltration of Itgb1^{+}Cd5^{+}Cd4^{+} T Cell Subsets in MAFLD

To further investigate the critical lymphocyte subsets that positively drive MAFLD, metabolic syndrome-associated MAFLD models (C57BL/6-Alms1-del) were established and enriched with high-quality NPCs for scRNA-seq to explore the heterogeneity of intrahepatic lymphocyte populations in the early stages of MAFLD (Figure 4a–e, Figure 5a–d, Supplementary Figure 5). After quality filtering, 73,470 cells (33,441 Onset; 40,029 MAFLD) were analyzed (Supplementary Figure 6). Increased T lymphocyte proportions were observed in MAFLD, with Cd5 expression restricted to T cell clusters (Figure 5e and f). T cells were stratified into seven subsets: Itgb1^{+}Cd4^{+}T cells, Cxcr6^{+}Cd4^{+}T cells, cytotoxic Cd8^{+}T cells, naïve Cd4^{+}T cells, naïve Cd8^{+}T cells, NKT cells, and γδ T cells. Cd5 was predominantly expressed in Itgb1^{+}Cd4^{+}T cells (Figure 5g–i), which lacked tissue-resident (Cxcr6, Ccr7) and memory T cell (Sell) markers but showed upregulated inflammatory genes (Tnfaip3, Cxcr4) in MAFLD (Figure 5i and j). GO/KEGG analyses revealed enrichment of this subset in cell migration/adhesion and T-cell activation pathways, confirming an early-activated effector phenotype (Figure 6a). GSEA demonstrated MAFLD-specific upregulation in Itgb1^{+}Cd5^{+}Cd4^{+} T cells of (1) chemokine adhesion

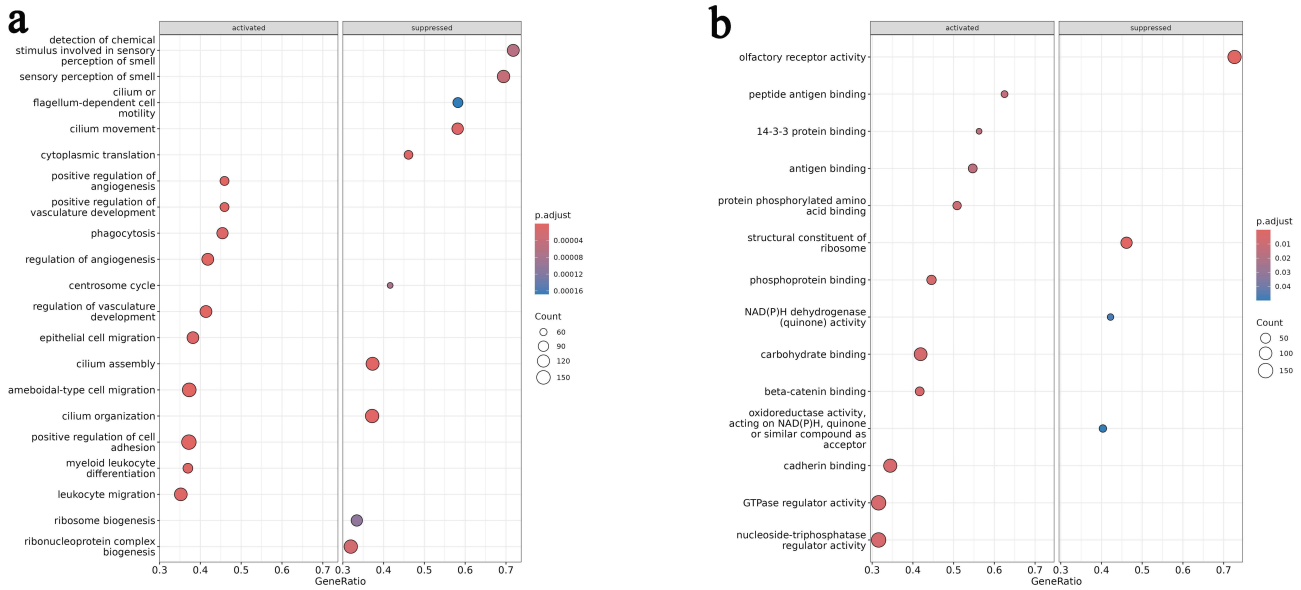

Figure 3 Integrated bulk RNA-seq and MR reveal hepatic trafficking of peripheral T lymphocytes in MAFLD pathogenesis. (**a**) GSEA of bulk RNA-seq data for differentially expressed genes associated with lymphocyte-related SNPs identified through GWAS and MR and the upregulated genes were significantly enriched in biological processes (BP) related to cell migration and motility, including "positive regulation of cell adhesion", "ameboidal-type cell migration", and "leukocyte migration". (**b**) GSEA revealed significant enrichment of upregulated genes in the molecular function (MF) term "cadherin binding".

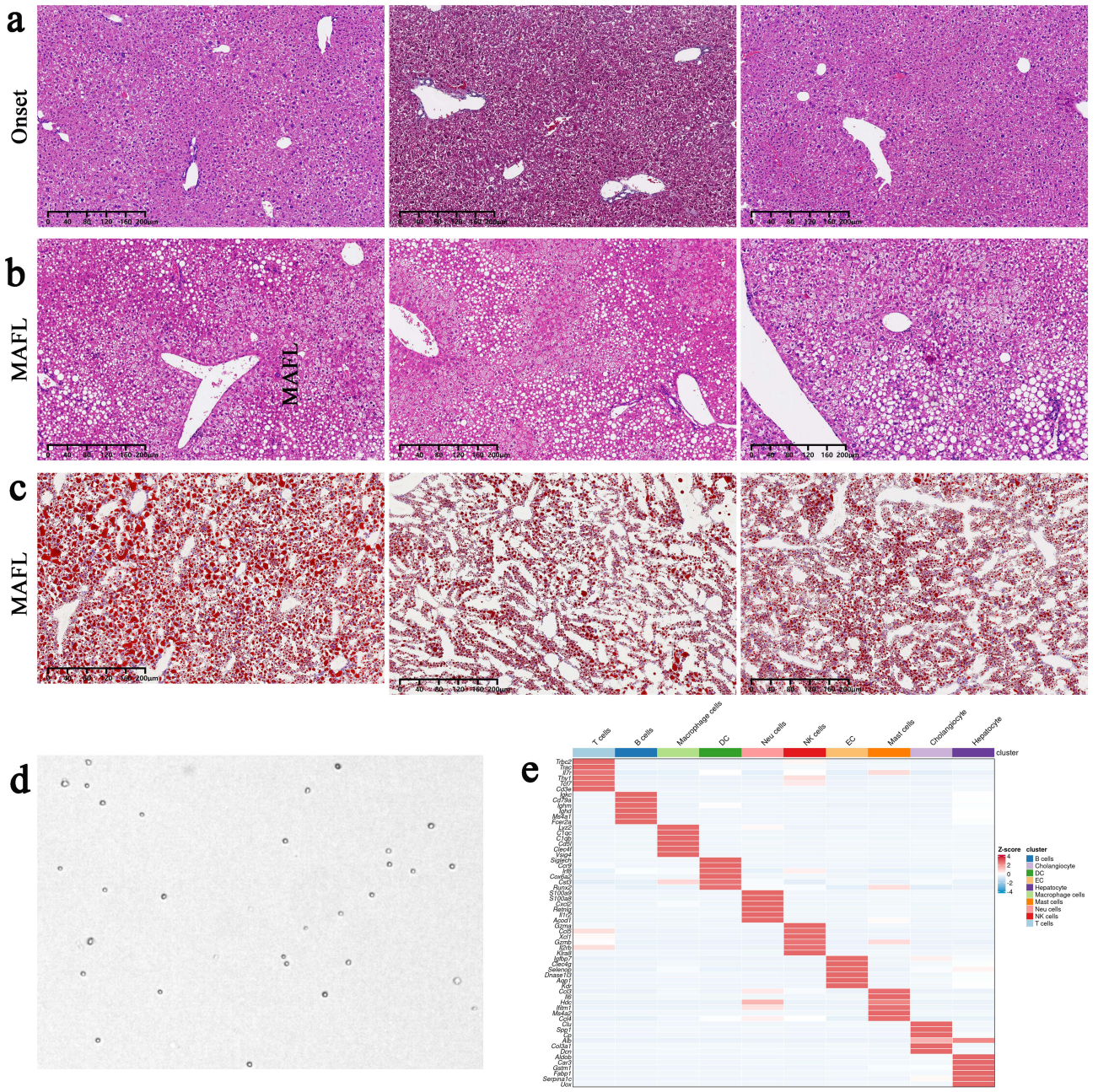

Figure 4 Pathological phenotypes of MAFLD mice with metabolic syndrome and quality control examples of liver non-parenchymal cells (NPCs), with disease and control groups analyzed in triplicate. (**a**). Liver Hematoxylin and Eosin staining (H&E staining) at the onset stage, showing well-preserved hepatocyte morphology with minimal microvesicular steatosis but no macrovesicular steatosis or intralobular inflammation. (**b**) Liver H&E staining at the MAFL stage, demonstrating macrovesicular steatosis involving >5% of hepatocytes, scattered inflammatory cell infiltration in some lobules, and preserved hepatic architecture without fibrosis, consistent with the MAFL stage. (**c**) Liver Oil Red O staining at the MAFL stage, revealing prominent red-stained lipid droplets within hepatic lobules. (**d**) All NPCs met stringent quality control criteria, including cell viability >90%, aggregation rate <5%, and minimal debris/impurities. (**e**) Heatmap of consensus NPC clustering based on transcriptomic profiles.

pathways, (2) NOTCH1-mediated cell communication, and (3) NRG1/TNF inflammatory signaling versus controls (Figure 6b), suggesting their role as pioneer effector T cells initiating MAFLD immunopathology.

Vcam1^{high} Kupffer Cells Mediate Hepatic Infiltration of Itgb1^{+}Cd5^{+}Cd4^{+} T Cells to Drive Inflammatory Responses

To elucidate mechanisms of Itgb1^{+}Cd5^{+}Cd4^{+} T cells infiltration, we interrogated intercellular communication networks. CellChat interaction analysis revealed that macrophages exhibited strong communication with T cells during early

https://doi.org/10.2147/JIR.S546860

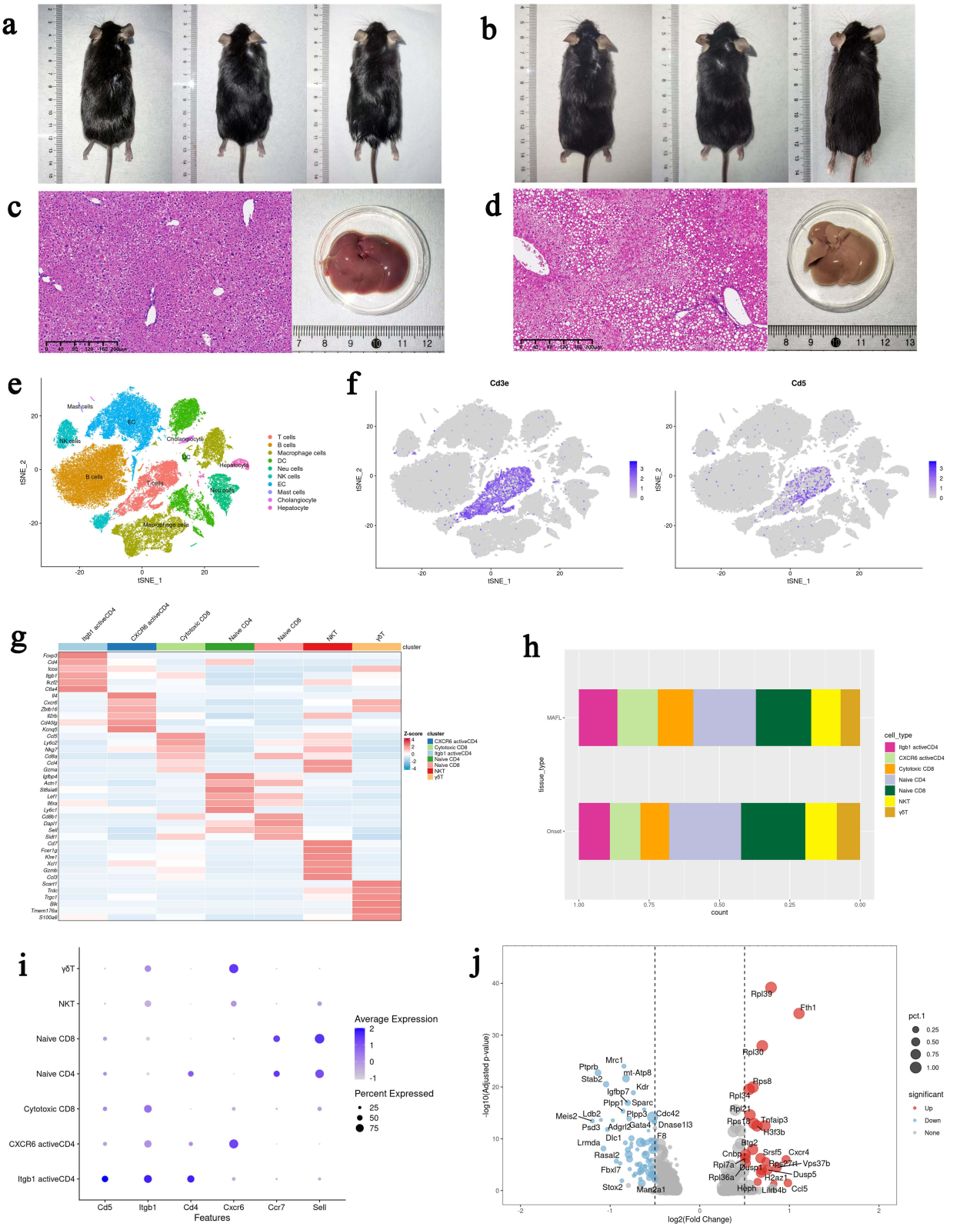

Figure 5 scRNA-seq reveals intrahepatic infiltration of Itgb1^{+}Cd5^{+}Cd4^{+} T-cell subsets during the early stages of MAFLD. (**a** and **b**) External photographs of mice at the Onset and MAFL stages showing abdominal obesity in MAFL-stage mice; (**c** and **d**) H&E-stained liver tissue sections and fresh liver specimens (without hepatic perfusion) from Onset and MAFL stages. MAFL-stage livers exhibit macrovesicular lipid deposition (black boxed areas in tissue sections), with mildly enlarged size and yellowish discoloration; (**e**) Integrated t-SNE plot of scRNA-seq data from both stages; (**f**) Cd5 is specifically enriched in hepatic T-cell populations, which were reclustered into six subsets; (**g**) Heatmaps illustrating overall clustering of intrahepatic non-parenchymal cells (NPCs) and T-cell subpopulations; (**h**) Activated Itgb1^{+}Cd4^{+} T-cell subsets show an increased proportion in the MAFL stage; (**i** and **j**) The Itgb1^{+}Cd4^{+}T-cell subset upregulates inflammation-related genes, including Tnfaip3 and Cxcr4, during the MAFL stage.

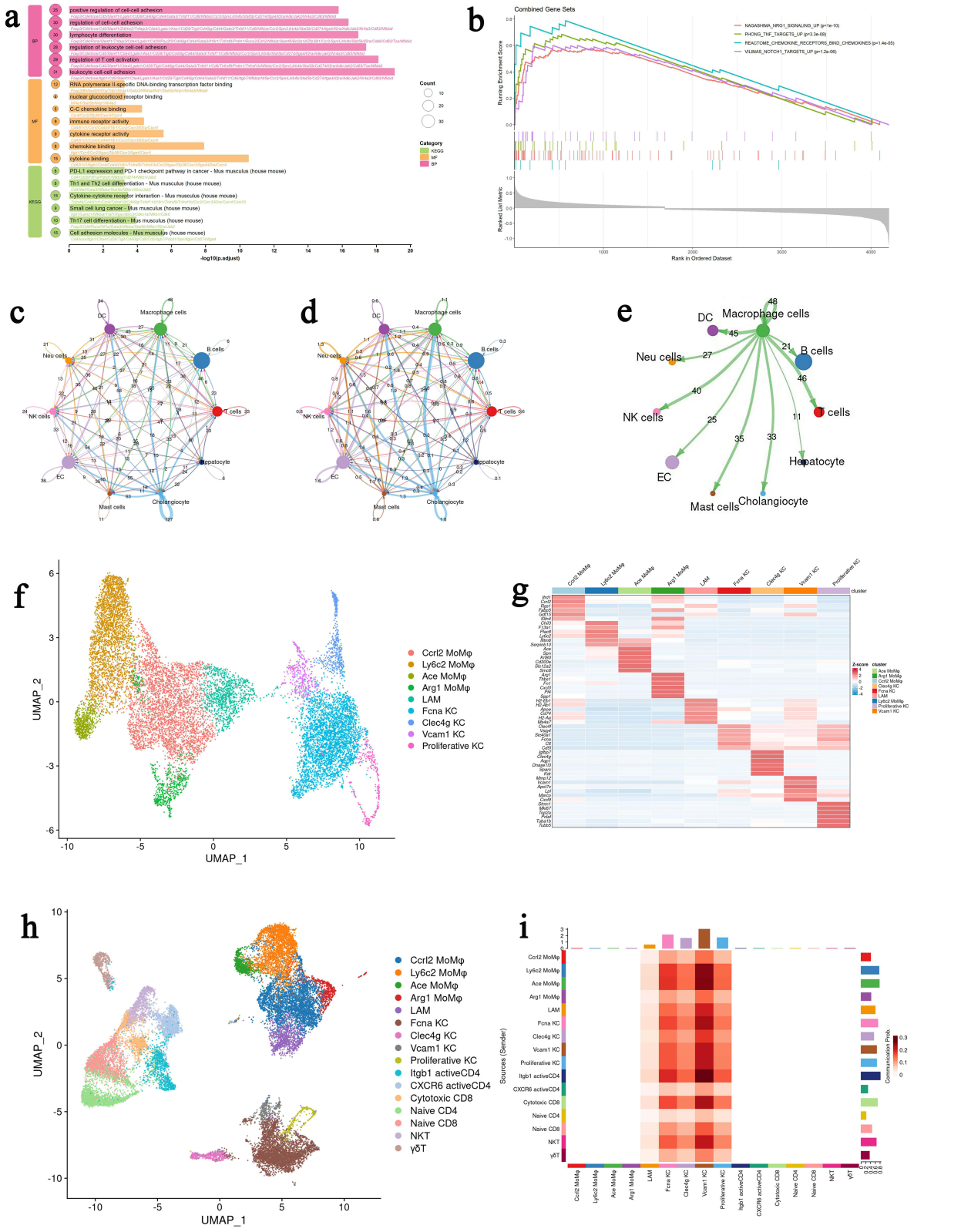

Figure 6 scRNA-seq reveals Vcam1^{high} Kupffer cell (KC)-mediated hepatic infiltration of Itgb1^{+}CD5^{+}CD4^{+} T cells, driving early inflammatory responses in MAFLD. (**a**) Gene Ontology and Kyoto Encyclopedia of Genes and Genomes enrichment analyses demonstrate that Itgb1^{+}Cd5^{+}Cd4^{+} T cells are enriched in pathways related to cell migration/adhesion and T-cell activation. (**b**) GSEA reveals upregulated pathways in MAFL-stage Itgb1^{+}Cd5^{+}Cd4^{+} T cells, including (1) chemokine adhesion pathways; (2) NOTCH1-mediated cell communication, and (3) NRG1/TNF inflammatory signaling. (**c–e**) Cell communication analysis indicates strong macrophage-T-cell interactions. (**f**) Macrophages were reclustered into four intrahepatic resident KC subsets and five peripherally derived monocyte-originated MoMφ subsets. (**g**). Heatmap of macrophage subpopulation clustering. (**h**) Integrated cell communication analysis between the nine macrophage subsets and seven T-cell subsets. (**i**) Vcam1^{high}KC cells exhibit significantly stronger Vcam1-Itgb1 ligand-receptor axis-mediated communication with Itgb1^{+}Cd5^{+}Cd4^{+} T cells compared to other macrophage subsets.

https://doi.org/10.2147/JIR.S546860

disease (Figure 6c–e, Supplementary Figure 7a and b), suggesting that macrophage subsets might orchestrate T cell recruitment. Macrophages were stratified into liver-resident Kupffer cells (KCs) and monocyte-derived macrophages (MoMφ), with further subclassification into Ccrl2$^+$ MoMφ, Ly6c2$^+$ MoMφ, Ace$^+$ MoMφ, Arg1$^+$ MoMφ, lipid-associated macrophages (LAM), Fcna$^+$ KC, Clec4g$^+$ KC, Vcam1^{high} KC, and proliferating KC (Figure 6f and g). Through CellChat communication analysis between macrophage subsets and T-cell subsets, mature liver-resident VCAM1^{high} KCs, characterized by high expression of matrix metalloproteinase-12 (Mmp12) and Cxcl9, were found to exhibit significantly stronger communication with Itgb1$^+$Cd5$^+$Cd4$^+$ T cells via the Vcam1-Itgb1 ligand-receptor axis compared to other macrophage subsets (Figure 6h and i, Supplementary Figure 7c). Mmp12 is a member of the matrix metalloproteinase family that plays a pivotal role in extracellular matrix (ECM) remodeling and tissue repair. These findings suggest Vcam1^{high} Mmp12$^+$KCs drive early hepatic inflammation not only via chemokine secretion but also through integrin-dependent Vcam1-Itgb1 interactions, enabling pathogenic infiltration of activated Itgb1$^+$Cd5$^+$Cd4$^+$T cells during MAFLD initiation. To further validate the conservation and generalizability of this axis, we analyzed a public scRNA-seq dataset of PBMCs from human MAFLD patients. We identified a corresponding population of peripheral Itgb1$^+$Cd5$^+$Cd4$^+$T cells, which was significantly expanded in MAFLD patients compared to healthy controls (32.8% vs 23.9%) (Figure 7a–c, Supplementary Figure 8a and b). Furthermore, we analyzed an independent scRNA-seq dataset from a non-genetically modified C57BL/6 mouse NASH model induced solely by a high-fat diet. In this independent model, we successfully identified both the Itgb1$^+$Cd5$^+$Cd4$^+$ T-cell subpopulation and Vcam1^{high} KCs (Figure 7d–g and Supplementary Figure 8c–h). Subsequent CellChat analysis confirmed that the interaction strength between these populations via the Vcam1-Itgb1 axis was significantly enhanced in NASH livers compared to controls (Figure 7h).

Discussion

This study integratively delineates the mechanistic link between peripheral Lympho and MAFLD through integrative multi-omics: (1) Bidirectional Mendelian randomization analysis established a unidirectional causal relationship between elevated peripheral lymphocyte count and increased MAFLD risk; (2) Mediation MR analysis further revealed that this causal effect is largely mediated through Cd5-driven inflammatory pathways; (3) By integrating MR instruments with human liver transcriptomic data, we found that this genetic predisposition coincides with the activation of lymphocyte hepatic homing and migration pathways; (4) ScRNA-seq in C57BL/6-Alms1-del model identified a novel liver-infiltrating Itgb1$^+$Cd5$^+$CD4$^+$ T cell subset, which interacts with hepatic Vcam1^{high}Mmp12$^+$ KCs via the Vcam1-Itgb1 ligand-receptor axis to drive early immune remodeling.; (5) Finally, we validated the conservation of this pathogenic cellular interaction in human PBMCs and an independent wild-type mouse model, confirming its relevance across species. MAFLD represents a multisystem metabolic-inflammatory disorder. Current diagnostic and prognostic standards remain reliant on invasive liver biopsy, with no validated non-invasive biomarkers.[23–25] Emerging evidence implicates hepatic innate and adaptive immune cells in maintaining immuno-metabolic homeostasis, suggesting immune signatures may sensitively track MAFLD progression.[17,26–28] Furthermore, the liver is not an isolated organ but actively communicates with extrahepatic tissues via systemic circulation, exchanging bioactive molecules and immune cells.[13,14,29] The cellular components of peripheral blood may theoretically mirror, to some extent, the immune dysregulation in MAFLD, suggesting their potential utility for non-invasive diagnosis and disease monitoring. Thus, clinical evaluation of MAFLD from an immunological perspective is etiologically justified. Emerging evidence demonstrates a close association between alterations in peripheral immune cells (particularly lymphocytes) and MAFLD progression, including activation of cytotoxic cells and Cd4$^+$ T cells, exhaustion of NK cells and Cd4$^+$ T cells, Th1/Th2/Th17 polarization of Cd4$^+$ T cells, and increased frequency of non-classical monocyte subsets.[17,30,31] However, prior studies have not thoroughly investigated whether a causal relationship exists between peripheral Lympho and MAFLD, nor the underlying mechanisms. To address this, MR analysis was performed on multiple circulating blood cell indices, identifying Lympho as the sole white blood cell parameter with a genetically predicted causal association with MAFLD. Given that alterations in certain leukocyte parameters may arise secondary to MAFLD development and acknowledging potential bidirectional causality between specific BCT and MAFLD, reverse MR analysis was performed on all leukocyte features and positive findings. However, no causal associations were observed between MAFLD and other leukocyte features except Lympho. This is likely due to the influence of other inflammatory cell confounders on the association between genetic variants and target

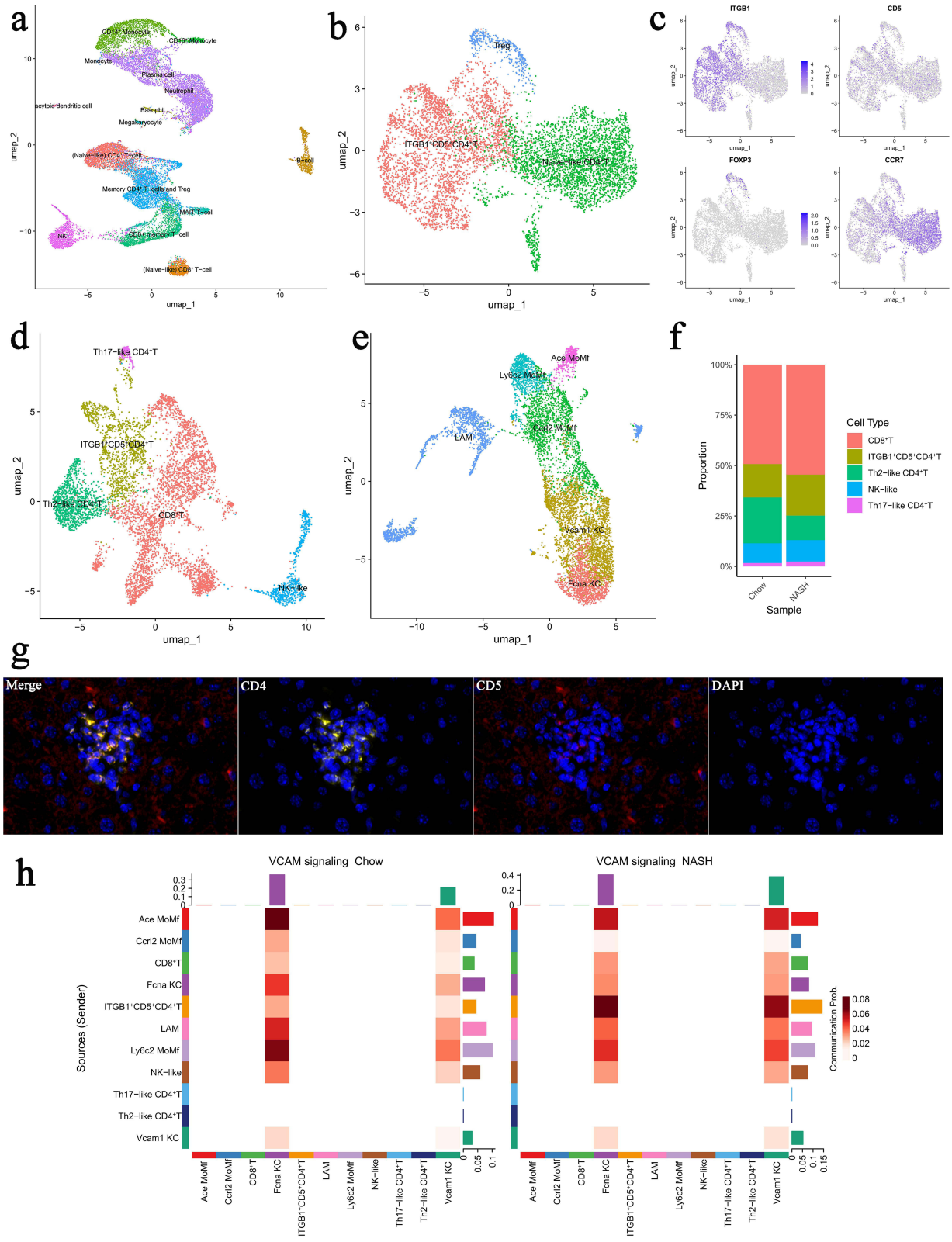

Figure 7 Validation of T Cell and Macrophage Subpopulations in Human PBMCs and an Independent Mouse Model. (**a**). UMAP projection of scRNA-seq data showing overall cellular composition in PBMCs from human MAFLD patients and healthy controls; (**b**) Identification of the Itgb1^{+}Cd5^{+}Cd4^{+} T cell subpopulation within clustered T cells from human PBMCs; (**c**) Expression patterns of target genes in T cell subpopulations from human PBMCs; (**d**) UMAP visualization of T cell subpopulations in the independent murine liver NPC scRNA-seq dataset, highlighting the Itgb1^{+}Cd5^{+}CD4^{+} T cell cluster; (**e**) UMAP visualization of macrophage subpopulations in the independent murine liver NPC scRNA-seq dataset, identifying the Vcam1^{high} KCs; (**f**) Comparative analysis of Itgb1^{+}Cd5^{+}Cd4^{+} T cell proportions between disease and control groups; (**g**) Multiplex immunofluorescence staining of liver sections from Alms1-del mice demonstrates focal aggregation of Cd5^{+}Cd4^{+} T cells during the MAFL stage; (**h**). CellChat analysis of the independent murine scRNA-seq dataset confirms enhanced communication strength between Vcam1^{high} KCs and Itgb1^{+}Cd5^{+}Cd4^{+} T cells mediated through the Vcam1-Itgb1 ligand-receptor axis.

https://doi.org/10.2147/JIR.S546860

traits. Although several cross-sectional studies have reported significant associations between MAFLD and alterations in the proportions or absolute counts of non-lymphocytic leukocytes,[32–34] these changes are likely confounded by disease progression and complex interactions among diverse cell populations involved in inflammatory responses.

Through mediational MR analysis, it was demonstrated that the causal effect of Lympho on MAFLD pathogenesis was partially mediated by the upregulation of membrane Cd5 expression. This positions Cd5 as a key immunoregulatory checkpoint, transducing peripheral immune activation into intrahepatic inflammation. Furthermore, previous studies have established that Cd5 plays a significant role in modulating T cell immune responses.[35] However, the MR-derived causal relationships and Cd5's immunomodulatory properties remained insufficient to establish whether peripheral Lympho actively triggers intrahepatic inflammation. Therefore, the potential of circulating lymphocytes was systematically investigated to directly orchestrate hepatic inflammatory onset.

By integrating bulk RNA-seq with MR analyses, lymphocyte-associated genetic loci were significantly enriched in cell migration and adhesion pathways. This finding not only supports the potential link between Cd5-mediated inflammatory pathways and lymphocyte migration but further suggests that the dynamic recruitment of peripheral lymphocytes to the liver may play a pivotal role in MAFLD pathogenesis. Compared to traditional cross-sectional studies, this work combines MR with transcriptional profiling to reveal the active migratory properties of peripheral lymphocytes, indicating their direct involvement in reshaping the intrahepatic immune microenvironment to drive disease progression. However, whether enhanced migratory capacity is sufficient to initiate an inflammatory response, as well as the underlying molecular effector mechanisms, remains to be further elucidated.

In this study, we employed male C57BL/6-Alms1-del mice fed a WD to model the spectrum of MAFLD. This model recapitulates not only human liver pathology but also extrahepatic manifestations, including chronic kidney disease (CKD) and cardiovascular disease (CVD), thereby closely mimicking human systemic metabolic syndrome.[20,36–38] Transcriptomic alignment analysis confirmed a significant correlation between this model and human MASH liver gene expression profiles, supporting its validity for investigating the entire disease course.[20] For the WD formulation, we used the GAN diet (D09100310 formula) containing 40% fat, 20% fructose, and 2% cholesterol, without pharmacological intervention. This dietary regimen has been demonstrated by recent studies to optimally replicate the nutritional etiology of human MASH.[21] For scRNA-seq, we specifically isolated liver non-parenchymal cells (NPCs) to avoid the transcriptional dominance of hepatocytes, which constitute the majority of the liver parenchyma. This enrichment strategy significantly enhances the sequencing depth and coverage for resident immune populations, thereby improving the resolution for identifying rare cell subsets and their low-expression genes. ScRNA-seq and cellular interaction analysis revealed specialized crosstalk between hepatic $Vcam1^{high}$ KCs and $Itgb1^{+}Cd5^{+}Cd4^{+}$ T cells via the Vcam1-Itgb1 ligand-receptor dyad. These findings functionally couple CD5 activity with migratory mechanisms, demonstrating its dual role in both potentiating T cell pro-inflammatory responses through activation pathways and facilitating hepatic stromal targeting via Itgb1-mediated adhesion signaling. Vcam1 is a cell adhesion molecule that maintains tissue architecture, mediates immune responses, and facilitates diverse cellular processes in multiple diseases.[39] Notably, this study provides the first evidence that the Vcam1-Itgb1 signaling pathway is associated with $Cd4^{+}$ T cell infiltration in the early stages of MAFLD. KCs, the resident macrophage subset in the liver, originate from yolk sac progenitors and are characterized by self-renewal capacity and immobility. Under steady-state conditions, KCs constitute the largest population of macrophages within the liver.[40] Previous studies have demonstrated that the population of resident KCs undergoes significant alterations during the progression of MAFLD,[41,42] wherein activated KCs secrete chemokines such as Ccl2 to recruit peripheral immune cells to the liver and promote MAFLD progression by producing pro-inflammatory cytokines, including tumor necrosis factor (TNF) and interleukin-1β (IL-1β).[43,44] This study reveals for the first time that $Vcam1^{high}$ KCs may drive inflammation through dual mechanisms: (1) $Vcam1^{high}$ KCs secrete Mmp12 to remodel the extracellular matrix, and (2) $Vcam1^{high}$ KCs recruit $Itgb1^{+}Cd5^{+}Cd4^{+}$ T cell subsets to the liver by providing adhesion anchoring sites through Vcam1-Itgb1 signaling, thereby establishing a pro-inflammatory microenvironment. Notably, $Itgb1^{+}Cd5^{+}Cd4^{+}$ T cells in incipient MAFLD exhibit marked upregulation of inflammatory mediators (Tnfaip3, Cxcr4) and TNF pathway activation, suggesting post-migratory perpetuation of

inflammatory cascades through cytokine-mediated stimulation of resident immune populations. This establishes a self-reinforcing "infiltration-retention-amplification" circuit that potentiates MAFLD progression.

While this study has several limitations persist: (1) Although sensitivity analyses and multivariable MR approaches were employed to mitigate horizontal pleiotropy and confounding, residual bias from unknown genetic factors or cell subset-specific effects cannot be fully excluded, despite retaining a substantial number of SNPs in our screening; (2) While early-stage MAFLD models were selected to isolate lymphocyte-driven disease mechanisms, the generalizability of these peripheral immunoregulatory pathways to advanced disease stages or comorbid metabolic contexts requires further validation; (3) Although scRNA-seq revealed interaction signatures between Itgb1^{+}Cd5^{+}Cd4^{+} T cells and Vcam1^{high} KCs, functional validation of Vcam1-Itgb1 axis-mediated T cell infiltration through gene knockout or blockade experiments remains essential. Future investigations should employ cross-organ single-cell atlas construction and spatiotemporal multi-omics integration to comprehensively map MAFLD-associated immunoregulatory networks.

Conclusion

In conclusion, Peripheral T lymphocytes exhibit a positive causal association with MAFLD development mediated by Cd5 expression levels, while liver-resident Vcam1^{high}Mmp12^{+} KCs may facilitate early immune microenvironment remodeling in MAFLD by recruiting Itgb1^{+}Cd5^{+}Cd4^{+} T cells via the Vcam1-Itgb1 pathway. These findings provide novel insights into the mechanistic link between peripheral and hepatic immune regulation.

Data Sharing Statement

The data supporting this study's findings are available on request from the corresponding author.

Author Contributions

All authors made a significant contribution to the work reported, whether that is in the conception, study design, execution, acquisition of data, analysis and interpretation, or in all these areas; took part in drafting, revising or critically reviewing the article; gave final approval of the version to be published; have agreed on the journal to which the article has been submitted; and agree to be accountable for all aspects of the work.

Funding

This research was supported by National High Level Hospital Clinical Research Funding (BJ-2023-083).

Disclosure

The authors report no conflicts of interest in this work.

References

1. Eslam M, Fan JG, Yu ML. et al. The Asian Pacific association for the study of the liver clinical practice guidelines for the diagnosis and management of metabolic dysfunction-associated fatty liver disease. *Hepatol Int*. 2025;19(2):261–301.
2. Singh A, Dhaliwal AS, Kumar A, et al. Awareness of nonalcoholic fatty liver disease is increasing but remains very low in a representative US cohort. *Dig Dis Sci*. 2020;65(4):978–986. doi:10.1007/s10620-019-05700-9
3. Targher G, Valenti L, Byrne CD. Metabolic Dysfunction-Associated Steatotic Liver Disease. *N Engl J Med*. 2025;393(7):683–698. doi:10.1056/NEJMra2412865
4. Peiseler M, Schwabe R, Hampe J, Kubes P, Heikenwälder M, Tacke F. Immune mechanisms linking metabolic injury to inflammation and fibrosis in fatty liver disease–novel insights into cellular communication circuits. *J Hepatol*. 2022;77(4):1136–1160. doi:10.1016/j.jhep.2022.06.012
5. Eslam M, Sanyal AJ, Mafld JG. A consensus-driven proposed nomenclature for metabolic associated fatty liver disease. *Gastroenterology*. 2020;158(7):1999–2014. doi:10.1053/j.gastro.2019.11.312
6. Martin OP, Wallace MS, Oetheimer C, et al. Single-cell atlas of human liver and blood immune cells across fatty liver disease stages reveals distinct signatures linked to liver dysfunction and fibrogenesis. *Nat Immunol*. 2025;26(9):1596–1611. doi:10.1038/s41590-025-02255-y
7. Younossi ZM, Zelber-Sagi S, Lazarus JV, et al. Global Consensus Recommendations for Metabolic Dysfunction-Associated Steatotic Liver Disease and Steatohepatitis. *Gastroenterology*. 2025;169(5):1017–1032. doi:10.1053/j.gastro.2025.02.044
8. Harrison SA, Bedossa P, Guy CD, et al. A Phase 3, Randomized, Controlled Trial of Resmetirom in NASH with Liver Fibrosis. *N Engl J Med*. 2024;390(6):497–509. doi:10.1056/NEJMoa2309000
9. Sanyal AJ, Newsome PN, Kliers I, et al. Phase 3 Trial of Semaglutide in Metabolic Dysfunction-Associated Steatohepatitis. *N Engl J Med*. 2025;392(21):2089–2099. doi:10.1056/NEJMoa2413258

10. He Y, Qian S, van Der Merwe S, et al. Immunopathogenic mechanisms and immunoregulatory therapies in MASLD. *Cell Mol Immunol*. 2025;22 (10):1159–1177. doi:10.1038/s41423-025-01307-5
11. Walsh SK, Mezzani I, Bermano G. Role of selenium and 17β oestradiol in modulating lipid accumulation in in vitro models of obesity and NAFLD. *Food Med Homol*. 2025;2(4):9420056. doi:10.26599/FMH.2025.9420056
12. Sun WL, Li XY, Dou HY, et al. Myricetin supplementation decreases hepatic lipid synthesis and inflammation by modulating gut microbiota. *Cell Rep*. 2021;36(9):109641. doi:10.1016/j.celrep.2021.109641
13. Wang F, So K-F, Xiao J, Wang H. Organ-organ communication: the liver's perspective. *Theranostics*. 2021;11(7):3317. doi:10.7150/thno.55795
14. Loomba R, Friedman SL, Shulman GI. Mechanisms and disease consequences of nonalcoholic fatty liver disease. *Cell*. 2021;184(10):2537–2564. doi:10.1016/j.cell.2021.04.015
15. Gehrke N, Schattenberg JM. Metabolic inflammation—a role for hepatic inflammatory pathways as drivers of comorbidities in nonalcoholic fatty liver disease? *Gastroenterology*. 2020;158(7):1929–1947. doi:10.1053/j.gastro.2020.02.020
16. Mu X, Zou J, Chen J, et al. Low platelets: a new and simple prognostic marker for patients with hepatitis E virus-related acute liver failure. *Hepatol Int*. 2022;16(5):1116–1126. doi:10.1007/s12072-022-10302-1
17. Lin S-Z, Fan J-G. Peripheral immune cells in NAFLD patients: a spyhole to disease progression. *EBioMedicine*. 2022;75:103768. doi:10.1016/j.ebiom.2021.103768
18. Sookoian S, Pirola CJ, Valenti L, Davidson NO. Genetic pathways in nonalcoholic fatty liver disease: insights from systems biology. *Hepatology*. 2020;72(1):330–346. doi:10.1002/hep.31229
19. Fairfield CJ, Drake TM, Pius R, et al. Genome-Wide Association Study of NAFLD Using Electronic Health Records. *Hepatol Commun*. 2022;6 (2):297–308. doi:10.1002/hep4.1805
20. Ganguly S, Muench GA, Shang L, et al. Nonalcoholic steatohepatitis and HCC in a hyperphagic mouse accelerated by western diet. *Cell Mol Gastroenterol Hepatol*. 2021;12(3):891–920. doi:10.1016/j.jcmgh.2021.05.010
21. Vacca M, Kamzolas I, Harder LM, et al. An unbiased ranking of murine dietary models based on their proximity to human metabolic dysfunction-associated steatotic liver disease (MASLD). *Nat Metab*. 2024;6(6):1178–1196. doi:10.1038/s42255-024-01043-6
22. Larsen FT, Hansen D, Terkelsen MK, et al. Stellate cell expression of SPARC-related modular calcium-binding protein 2 is associated with human non-alcoholic fatty liver disease severity. *JHEP Rep*. 2023;5(2):100615. doi:10.1016/j.jhepr.2022.100615
23. Harrison SA, Ratziu V, Boursier J, et al. A blood-based biomarker panel (NIS4) for non-invasive diagnosis of non-alcoholic steatohepatitis and liver fibrosis: a prospective derivation and global validation study. *Lancet Gastroenterol Hepatol*. 2020;5(11):970–985. doi:10.1016/S2468-1253(20)30252-1
24. Newsome PN, Sasso M, Deeks JJ, et al. FibroScan-AST (FAST) score for the non-invasive identification of patients with non-alcoholic steatohepatitis with significant activity and fibrosis: a prospective derivation and global validation study. *Lancet Gastroenterol Hepatol*. 2020;5 (4):362–373. doi:10.1016/S2468-1253(19)30383-8
25. Vilar-Gomez E, Chalasani N. Non-invasive assessment of non-alcoholic fatty liver disease: clinical prediction rules and blood-based biomarkers. *J Hepatol*. 2018;68(2):305–315. doi:10.1016/j.jhep.2017.11.013
26. Sutti S, Albano E. Adaptive immunity: an emerging player in the progression of NAFLD. *Nat Rev Gastroenterol Hepatol*. 2020;17(2):81–92. doi:10.1038/s41575-019-0210-2
27. Lin S-Z, Xie Y, Cheng Y-Q, et al. C/EBPβ-VCAM1 axis in Kupffer cells promotes hepatic inflammation in MASLD. *JHEP Rep*. 2025;7(8):101418. doi:10.1016/j.jhepr.2025.101418
28. Liu J, Ding M, Bai J, et al. Decoding the role of immune T cells: a new territory for improvement of metabolic-associated fatty liver disease. *Imeta*. 2023;2(1):e76. doi:10.1002/imt2.76
29. Fuchs A, Samovski D, Smith GI, et al. Associations among adipose tissue immunology, inflammation, exosomes and insulin sensitivity in people with obesity and nonalcoholic fatty liver disease. *Gastroenterology*. 2021;161(3):968–981. doi:10.1053/j.gastro.2021.05.008
30. DuPage M, Bluestone JA. Harnessing the plasticity of CD4(+) T cells to treat immune-mediated disease. *Nat Rev Immunol*. 2016;16(3):149–163. doi:10.1038/nri.2015.18
31. Nguyen QP, Deng TZ, Witherden DA, Goldrath AW. Origins of CD4(+) circulating and tissue-resident memory T-cells. *Immunology*. 2019;157 (1):3–12. doi:10.1111/imm.13059
32. Liu C-F, Chien L-W. Predictive role of neutrophil-percentage-to-albumin ratio (NPAR) in nonalcoholic fatty liver disease and advanced liver fibrosis in nondiabetic US adults: evidence from NHANES 2017–2018. *Nutrients*. 2023;15(8):1892. doi:10.3390/nu15081892
33. Chen G, Fan L, Yang T, et al. Prognostic nutritional index (PNI) and risk of non-alcoholic fatty liver disease and advanced liver fibrosis in US adults: evidence from NHANES 2017–2020. *Heliyon*. 2024;10(4):e25660. doi:10.1016/j.heliyon.2024.e25660
34. Gadd VL, Patel PJ, Jose S, Horsfall L, Powell EE, Irvine KM. Altered peripheral blood monocyte phenotype and function in chronic liver disease: implications for hepatic recruitment and systemic inflammation. *PLoS One*. 2016;11(6):e0157771. doi:10.1371/journal.pone.0157771
35. He M, Roussak K, Ma F, et al. CD5 expression by dendritic cells directs T cell immunity and sustains immunotherapy responses. *Science*. 2023;379 (6633):eabg2752. doi:10.1126/science.abg2752
36. Girard D, Petrovsky N. Alström syndrome: insights into the pathogenesis of metabolic disorders. *Nat Rev Endocrinol*. 2011;7(2):77–88. doi:10.1038/nrendo.2010.210
37. Farrell GC, Mridha AR, Yeh MM, et al. Strain dependence of diet-induced NASH and liver fibrosis in obese mice is linked to diabetes and inflammatory phenotype. *Liver Int*. 2014;34(7):1084–1093. doi:10.1111/liv.12335
38. Arsov T, Silva DG, O'Bryan MK, et al. Fat aussie–a new Alström syndrome mouse showing a critical role for ALMS1 in obesity, diabetes, and spermatogenesis. *Mol Endocrinol*. 2006;20(7):1610–1622. doi:10.1210/me.2005-0494
39. Wang L, Tang Y, Tang J, et al. Endothelial cell-derived extracellular vesicles expressing surface VCAM1 promote sepsis-related acute lung injury by targeting and reprogramming monocytes. *J Extracell Vesicles*. 2024;13(3):e12423. doi:10.1002/jev2.12423
40. Guilliams M, Scott CL. Liver macrophages in health and disease. *Immunity*. 2022;55(9):1515–1529. doi:10.1016/j.immuni.2022.08.002
41. Daemen S, Gainullina A, Kalugotla G, et al. Dynamic shifts in the composition of resident and recruited macrophages influence tissue remodeling in NASH. *Cell Rep*. 2021;34(2):108626. doi:10.1016/j.celrep.2020.108626
42. Blériot C, Barreby E, Dunsmore G, et al. A subset of Kupffer cells regulates metabolism through the expression of CD36. *Immunity*. 2021;54 (9):2101–2116. doi:10.1016/j.immuni.2021.08.006

43. Dixon LJ, Berk M, Thapaliya S, Papouchado BG, Feldstein AE. Caspase-1-mediated regulation of fibrogenesis in diet-induced steatohepatitis. *Lab Invest*. 2012;92(5):713–723. doi:10.1038/labinvest.2012.45
44. Okina Y, Sato-Matsubara M, Matsubara T, et al. TGF-β1-driven reduction of cytoglobin leads to oxidative DNA damage in stellate cells during non-alcoholic steatohepatitis. *J Hepatol*. 2020;73(4):882–895. doi:10.1016/j.jhep.2020.03.051